POLITECNICO MILANO 1863

SCUOLA DI INGEGNERIA INDUSTRIALE E DELL'INFORMAZIONE

Executive Summary of the Thesis

Development of a reduced-order model of a non-uniform distortion screen and re-staggered inlet guide vane

Laurea Magistrale in Mechanical Engineering - Ingegneria Meccanica

Author: Alessandro Nardone

Advisor: Prof. Paolo Gaetani

Co-advisor: Prof. Fabrizio Fontaneto

Academic year: 2025-2026

1. Introduction

Future aircraft propulsion systems are being developed to meet ambitious environmental targets, including substantial reductions in CO_2 and NO_x emissions. Promising concepts such as Boundary Layer Ingestion (BLI), Short Nacelle High Bypass (SNHB) turbofans, and open-rotor architectures improve efficiency but introduce significant inlet flow distortion. Unlike conventional engines, these configurations are expected to operate continuously under distorted inflow conditions, making distortion a critical design challenge.

Prior to the present work, experimental investigations conducted at the VKI R4 compressor facility demonstrated that realistic total-pressure distortions can significantly degrade compressor performance and operability. A promising mitigation strategy is the circumferential re-staggering of Inlet Guide Vanes (IGV), which aims to restore the rotor incidence distribution. However, the non-uniform IGV stagger also modifies the upstream flow field, creating complex interactions with the distortion screen. The analysis of this interaction currently requires expensive full-annulus CFD simulations.

Building on these results, the present work develops a predictive low-order model of the coupled flow redistribution generated by a non-uniform distortion screen and a non-uniformly re-staggered IGV row, together with the dedicated CFD simulations used to support and validate it.

Objectives

- Characterise circumferential flow redistribution through a non-uniform total-pressure distortion screen and identify the governing parameters.
- Investigate the aerodynamic interaction between a distortion screen and a non-uniformly re-staggered IGV row as a function of their axial spacing.
- Develop a low-order model to predict the circumferential flow field generated by the coupled Screen–IGV system.
- Propose a preliminary IGV re-staggering strategy based on model predictions.

To achieve these objectives, a dual-screen model was first developed, treating the IGV row as an equivalent aerodynamic resistance. The model aims to provide a computationally efficient tool for distortion-screen design and for the development of IGV re-staggering strategies aimed at mitigating compressor distortion effects.

2. Numerical and Experimental Methodology

Experimental setup

The experimental campaign was conducted, prior to the present work, on the VKI closed-loop high-speed compressor test rig R4 [5]. The test section installed within R4 is the DREAM compressor, designed by Safran Aero Boosters as a highly loaded research stage representative of next-generation boosters. The DREAM test section is a 1.5-stage configuration comprising an Inlet Guide Vane (IGV) row with 100 blades, a rotor with 76 blades, and a stator with 100 blades. A cross-sectional view of the stage is shown in Figure 1.

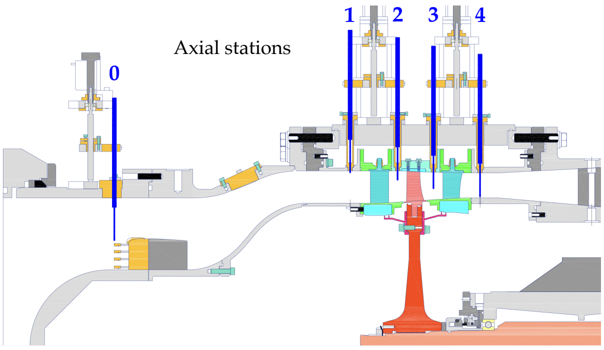

Figure 1: Cross-sectional view of the DREAM test section with the five axial measurement planes: 0 (stage inlet), 1 (IGV inlet), 2 (IGV outlet / rotor inlet), 3 (rotor outlet / stator inlet), 4 (stage outlet).

Distortion screen

The inlet total pressure distortion is generated by a non-uniform wire mesh screen placed one IGV axial chord upstream of the IGV leading edge, at Plane 1. The screen replicates the fan outlet total pressure profile of an ultra-high bypass ratio turbofan operating in crosswind conditions. The distortion is assumed to be purely circumferential, with no radial variation.

The screen is subdivided into six circumferential sectors defined by four distinct wire mesh configurations (W0, W1, W2, W3), characterised by their wire diameter d_w, aperture w, mesh count n, and porosity β, as summarised in Table 1. The resulting screen geometry is shown in Figure 2a.

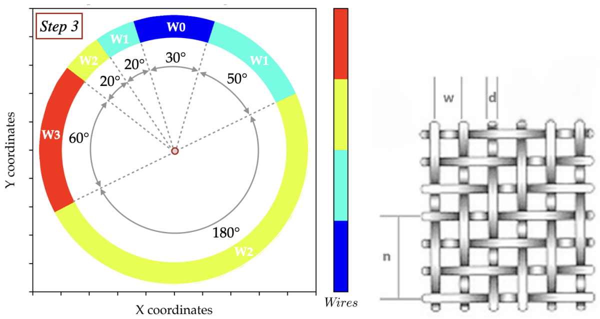

(a) (b)

Figure 2: (a) Screen sector layout. (b) Wire mesh geometry

	W0 (clean)	W1	W2	W3
d_w [mm]	–	1.2	0.6	0.6
w [mm]	–	5.150	1.940	1.517
n	–	4	10	12
β	–	0.66	0.58	0.51

Table 1: Geometric parameters of the four wire mesh configurations.

The screen is installed at a normalised axial distance from the IGV of:

$$\Delta X_{\text{adim}} = \Delta X / D_m = 0.206, \qquad (1)$$

where D_m is the mean annulus diameter. This parameter governs the extent to which the upstream potential field of the IGV can reach the screen plane and perturb the redistribution it drives.

CFD Setup

A series of two-dimensional CFD simulations were carried out in ANSYS Fluent to validate the analytical model and provide physical insight into the flow redistribution mechanisms. The annular duct is unrolled into a planar channel, with periodic boundary conditions on the top and bottom faces making the simulation physically equivalent to a full 360° annular computation. The domain is split at the screen plane into an upstream block of length H and a downstream block of length $2H$, where H is the total circumferential length. Boundary conditions and domain geometry are illustrated in Figure 3: a uniform total pressure $P_t = 116\,820$ Pa and total temperature $T_t = 293.05$ K are imposed at the inlet, a prescribed mass flow rate at the outlet, and a circumferentially non-uniform porous jump at $X = H$.

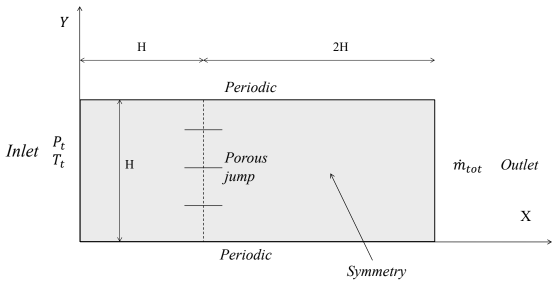

Figure 3: Two-dimensional CFD domain geometry and boundary conditions.

The distortion screen is modelled as a *porous jump* boundary condition in ANSYS Fluent, representing it as an infinitely thin actuator disk imposing a prescribed static pressure drop. The Fluent formulation expresses the pressure drop as:

$$\Delta p_s = -\left(C \cdot \tfrac{1}{2}\rho v^2\right)\Delta m, \tag{2}$$

where v is the face-normal velocity, ρ the local density, Δm the nominal porous medium thickness, and C the inertial resistance coefficient. A distinct value of C is assigned to each circumferential sector to reflect its wire mesh properties, mapped from the analytical total pressure loss coefficient K_c via isentropic relations. All simulations use a pressure-based coupled solver with air as a compressible ideal gas, second-order upwind spatial discretisation, and the SST k–ω turbulence model to capture shear-layer mixing downstream of the screen.

The mesh is structured quadrilateral, with axial refinement concentrated near the screen plane. A GCI study confirmed that this biased refinement outperforms a uniform mesh, yielding negligible discretisation uncertainty, and was therefore adopted for all simulations.

3. Single Screen Model

The annular duct is discretised into four independent stream tubes, one per distinct wire mesh configuration (W0–W3). Four axial stations are defined along every stream tube: a *far-upstream* plane where the static pressure is circumferentially uniform, a *screen-upstream* plane immediately upstream of the distortion screen, a *screen-downstream* plane immediately behind the screen, and a *far-downstream* plane where static pressure has fully re-equalised. A schematic of the multi-station, multi-segment domain is shown in Figure 4.

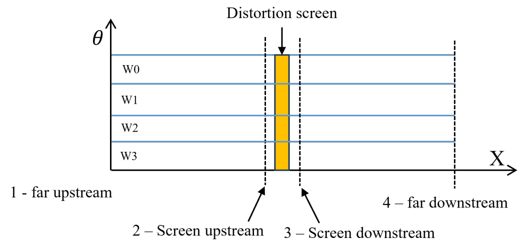

Figure 4: Analytical model schematics. θ, X = circumferential and axial directions.

The following hypotheses are adopted in the model: (1) losses are generated only by the screen and are modelled through empirical correlations; (2) each stream tube is treated as an independent one-dimensional channel; (3) steady state flow; (4) the inlet total pressure is circumferentially uniform; (5) the far-downstream static pressure is circumferentially uniform; (6) the screen is axially thin; (7) **the antisymmetric static-pressure condition**; (8) zero swirl angle; and (9) calorically perfect gas.

The system closure is provided by the **antisymmetric static-pressure condition**, which constitutes the key modelling hypothesis of this work. The model imposes that the arithmetic mean of the upstream and downstream static pressures be circumferentially uniform across all sectors:

$$\frac{P_{s,2,i} + P_{s,3,i}}{2} = \overline{P}_{\text{avg}}, \quad \forall i. \tag{3}$$

Here, $\overline{P}_{\text{avg}}$ is not an imposed value but is calculated by the model. This condition, initially

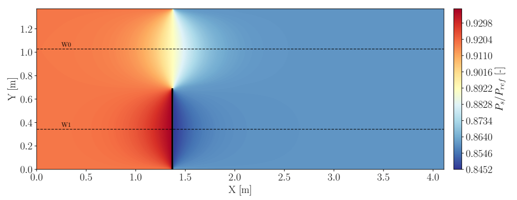

Figure 5: 2D colour map of normalised static pressure P_s/P_{ref} in the X–Y (axial-circumferential) plane; the black line marks the distortion screen

introduced by Gillespie [2], reflects the physical observation that the static pressure increases upstream of the distorted sector, and does not equalize immediately downstream. Its validity is confirmed by a CFD simulation on a simplified two-sector geometry: the normalised static pressure colour map in Figure 5 reveals a clear spatial antisymmetry between the upstream and downstream pressure fields in the distorted sector, consistent with Equation (3).
The total pressure loss across each sector is decomposed into three independent contributions:

$$K_c = G(\beta) \cdot F(Re_d) \cdot f_M(M), \tag{4}$$

where $G(\beta)$ is the porosity function, $F(Re_d)$ accounts for viscous and inertial forces, and $f_M(M)$ is the compressibility correction of Pinker [4]. A parametric analysis has been performed over four porosity functions (G_1–G_4) and eight Reynolds-number correlations. The model prediction has been compared to the experimental total pressure profiles from seven operating conditions to identify the best-fit configuration, which has a minimum RMSRE of 1.08%.
The governing equations are non-linear and strongly coupled; the system is therefore solved iteratively. Each iteration (i) applies isentropic relations at Station 2 to update thermodynamic quantities and sector mass flows from the current Mach number, T_t, P_t; (ii) evaluates the loss coefficient $K_{c,i}$ and computes Station 3 conditions; and (iii) updates all sectors' Station 2 Mach numbers simultaneously using proportional corrections derived from the residuals of the antisymmetric pressure constraint and the global mass-flow constraint. Convergence is reached when both residuals fall below 10^{-7}. A second loop enforces full static-pressure equalisation and stream-tube area consistency at the far-downstream Station 4.
The analytical model is compared against a full two-dimensional CFD solution for the single-screen configuration. The agreement is excellent across all three quantities and all four axial stations, with RMSRE values of 0.01% for total pressure, 0.08% for static pressure, and 0.33% for Mach number. The largest pointwise error (+1.60% in Mach number at the screen-upstream station of sector W0) is attributed to the discrete nature of the one-dimensional representation versus the smooth continuous CFD profiles.
The model is validated against seven experimental operating conditions measured at Plane 1 (immediately downstream of the screen). Since the physical measurement plane lies within the pressure relaxation region between Station 3 and Station 4, a linear interpolation at 70% of the inter-station distance is performed. Figure 6 shows the resulting circumferential distributions of P_t/P_{t0M}, P_s/P_{t0M} and Mach number for a representative operating condition.

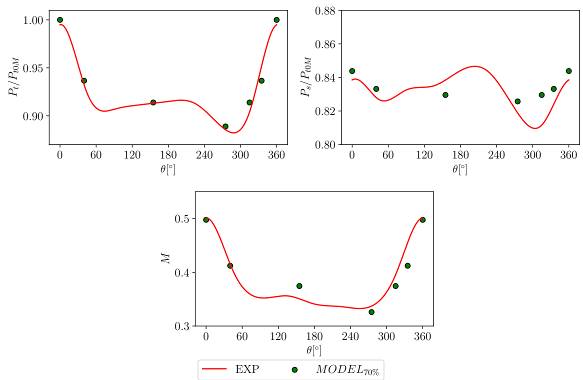

Figure 6: Circumferential distributions of P_t/P_{t0M}, P_s/P_{t0M}, Mach number at Plane 1. Red solid line: experimental data; green filled circles: analytical model interpolated.

The interpolated model reproduces the experimental total pressure, static pressure, and Mach number distributions with good accuracy, with RMSRE values of 0.82%, 1.14%, and 5.01% respectively. Residual discrepancies arise from two sources: the compressor back-pressure modifying the local static pressure upstream of the IGV (not captured by the single-screen model), and the non-negligible swirl angle present in the measurements, which is excluded by the zero-swirl hypothesis of the model.

4. Dual Screen Model

Since the re-staggered IGV row acts on the flow as an aerodynamic resistance, it is first modelled as a second distortion screen. The analytical model was extended to evaluate the aerodynamic interaction of two distortion screens placed in series. The modelling strategy diverges depending on the axial separation (ΔX_{adim}) between the two screens, non-dimensionalised with the annular mean diameter. Two limiting physical formulations were developed:

- **Coupled model:** Assumes the screens are sufficiently close that their pressure fields interact directly, sharing a single flow redistribution mechanism. A single global antisymmetric static pressure constraint bridges the entire two-screen assembly.
- **Decoupled model:** Assumes the screens are far apart. The upstream potential effect of the second screen does not affect the first one. The model acts as two successive, independent applications of the single screen solver.

An extensive error analysis against dual-screen CFD simulations across a sweep of axial distances revealed that neither model is universally valid (Figure 7). The Coupled model succeeds when the screens are nearly adjacent ($\Delta X \approx 0$) but its error grows exponentially as the distance increases. Conversely, the Decoupled model is accurate only for well-separated screens ($\Delta X_{\text{adim}} > 0.7$).

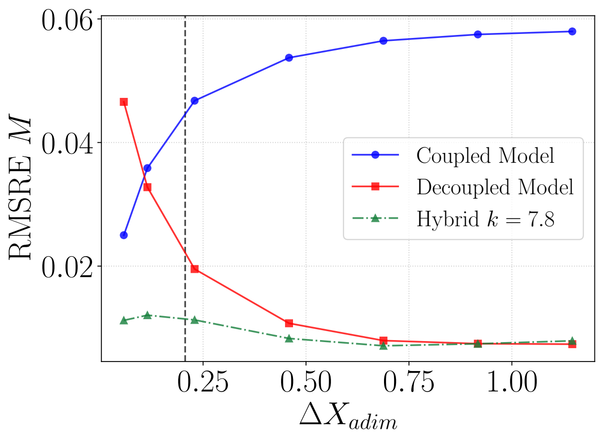

Figure 7: RMSRE for Mach number as a function of the inter-screen distance ΔX for the three models: Coupled, Decoupled, Hybrid.

To correctly model the intermediate region, where neither one of the two models achieved low RMSRE, a **Hybrid Model** was constructed. Using an exponentially decaying interpolation weighting function of the normalised axial distance, governed by a shape parameter k, the Hybrid model seamlessly transitions between the Coupled and Decoupled models. It computes a weighted average of the flow state variables from the two base models. As shown in Figure 7, it successfully reduces the error across all axial distances, matching the low error of the Coupled model at small distances and the Decoupled model at large distances, while maintaining a uniformly low error plateau in the intermediate range.

5. Screen–IGV Model

The Screen–IGV model extends the dual-screen formulation by replacing the second resistive element with an active blade row, the Inlet Guide Vane (IGV). Its full mathematical structure is preserved, while the loss model is substituted with the IGV loss and deviation correlations: the Lieblein [3] profile-loss correlation for the total pressure loss coefficient and the Carter [1] rule for the exit deviation angle, extended by Lieblein [3] for off-design incidence conditions. Since the loss correlation depends on outlet conditions, the problem is solved iteratively. The model is validated against a steady full-annulus RANS simulation with the screen at its nominal position and the IGV at uniform stagger, comparing sector-averaged profiles extracted from the CFD. Among the three models, the Hybrid model provides the best agreement, lowering the Mach-number RMSRE at the IGV outlet from 4.7% and 6.3% (Decoupled and Coupled models) to 3.0%, with total pressure reproduced almost exactly (RMSRE = 0.04%); the main discrepancy between CFD and model is a $\approx 2°$ flow angle error at the IGV outlet, attributed to the mean-line deviation correlation.

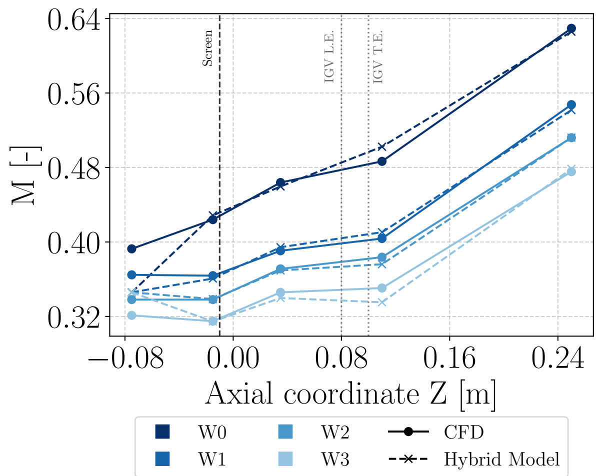

Figure 8: Sector-averaged Mach number M vs. axial coordinate Z: Hybrid model vs. CFD for sectors W0–W3.

Given an IGV stagger distribution around the annulus, the Screen–IGV model computes the incidence on the compressor rotor blades downstream of the IGV. The model is adapted to find the IGV re-staggering pattern which brings the rotor incidence to the design value $\iota_{\text{des}} = 1.40°$ across all circumferential sectors. The re-staggering pattern is optimised with a Powell hybrid root-finder, giving the optimal stagger distribution $\boldsymbol{\gamma}^{\star} = [-22.5, -9.8, 0.2, 16.8]°$. The velocity triangles at the rotor inlet are shown in Figure 9. Being single-objective, the procedure recovers the incidence exactly but leaves the Mach-number uncorrected, whose simultaneous control would require an additional design variable.

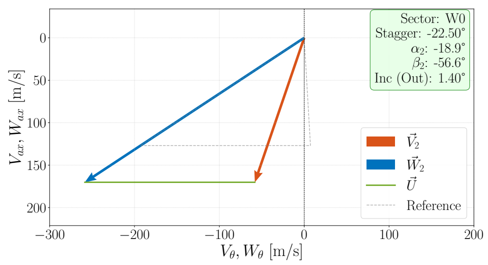

(a) W0 (clean)

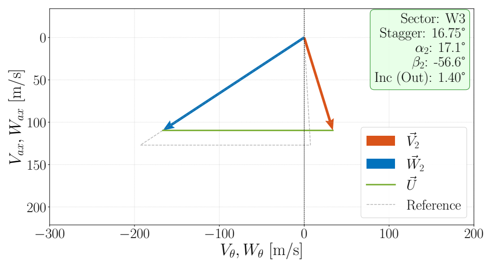

(b) W3 (most distorted)

Figure 9: Rotor velocity triangles after the IGV stagger optimisation.

6. Conclusions

From the work, many physical insights into the redistribution mechanism emerge. The circumferential redistribution induced by a non-uniform screen is established mostly upstream of it, where the blockage of the distorted sectors raises the static pressure and lowers the Mach number while the clean sector accelerates; a CFD model prescribing only the downstream total pressure therefore cannot recover the correct flow field, and the upstream region must be resolved explicitly. The antisymmetric closure hypothesis proves to be a valid condition to capture the redistribution on both sides of the element. Lastly, the back-pressure perturbation exerted by a downstream element on an upstream one relaxes exponentially with the axial spacing, making the transition from the coupled to the decoupled regime itself exponential and justifying the exponential weighting of the *Hybrid* model.

The priority for the future work is to validate the Screen–IGV model against CFD simulations of a non-uniformly re-staggered IGV row, which would produce stronger tangential gradients. The predicted optimal stagger vector for the four circumferential sectors, $\boldsymbol{\gamma}^{\star} = [-22.5, -9.8, 0.2, 16.8]°$, should then be validated both numerically and experimentally. Finally, a further modelling step is the coupling of each annular sector to its own operating point on the compressor map, accounting for the spatially non-uniform back-pressure that propagates upstream.

References

[1] Alfred DS Carter. The low speed performance of related aerofoils in cascade. 1950.

[2] John Gillespie, Andrew Hayden, Todd Lowe, Alexandrina Untaroiu, and Chase Nessler. Analysis of complex total pressure distortion screens using one-dimensional loss data. *Journal of Turbomachinery*, 147(10):101009, 2025.

[3] Seymour Lieblein. Loss and stall analysis of compressor cascades. *Journal of basic engineering*, 81(3):387–397, 1959.

[4] RA Pinker and MV Herbert. Pressure loss associated with compressible flow through square-mesh wire gauzes. *Journal of Mechanical Engineering Science*, 9(1):11–23, 1967.

[5] Riccardo Toracchio. Performance and stability analysis of a highly-loaded low-pressure compressor under distorted inflow conditions. 2024.